Contrib Mineral Petrol (2003) 145: 301–315
DOI 10.1007/s00410-003-0454-1

ORIGINAL PAPER

Chunjing Wei · Roger Powell

Phase relations in high-pressure metapelites in the system KFMASH (K_2O–FeO–MgO–Al_2O_3–SiO_2–H_2O) with application to natural rocks

Received: 22 March 2002 / Accepted: 7 January 2003 / Published online: 26 March 2003

Abstract Using a previously published, internally consistent thermodynamic dataset and updated models of activity–composition relations for solid solutions, petrogenetic grids in the model system KFMASH (K_2O–FeO–MgO–Al_2O_3–SiO_2–H_2O) and the subsystems KMASH and KFASH have been calculated with the software THERMOCALC 3.1 in the P–T range 5–36 kbar and 400–810 °C, involving garnet, chloritoid, biotite, carpholite, talc, chlorite, staurolite and kyanite/sillimanite with phengite, quartz/coesite and H_2O in excess. These grids, together with calculated AFM compatibility diagrams and pseudosections, are shown to be powerful tools for delineating the phase equilibria and P–T conditions of pelitic high-P assemblages for a variety of bulk compositions. The calculated equilibria and mineral compositions are in good agreement with petrological observation. The calculation indicates that the typical whiteschist assemblage kyanite–talc is restricted to the rocks with extremely high X_{Mg} values, decreasing X_{Mg} in a bulk composition favoring the stability of chloritoid and garnet. Also, the chloritoid–talc paragenesis is stable over 19–20 kbar in a temperature range of ca. 520–620 °C, being more petrologically important than the previously highlighted assemblage talc–phengite. Moreover, contours of the calculated Si isopleths in phengite in P–T and P–X pseudosections for different bulk compositions extend the experimentally derived phengite geobarometers to various KFMASH assemblages.

C. Wei (✉)
School of Earth and Space Sciences,
Beijing University, 100871 Beijing, China
E-mail: cjwei@pku.edu.cn
Tel.: +86-10-62754157
Fax: +86-10-62751159

R. Powell
School of Earth Sciences,
The University of Melbourne, 3052 Parkville, Australia

Editorial responsibility: B. Collins

Introduction

The model system KFMASH (K_2O–FeO–MgO–Al_2O_3–SiO_2–H_2O) has been successfully employed for metapelites in a number of classic studies (Thompson 1957), and has been used for the development of petrogenetic grids based on observations of natural mineral parageneses and experimental data (e.g., Albee 1965; Hess 1969; Harte 1975; Harte and Hudson 1979; Labotka 1981; Holdaway et al. 1982). More recently, the use of mineral thermodynamic databases has led to the construction of quantitative petrogenetic grids for this system which have greatly extended the applicability of such model systems to natural rock assemblages for low- and medium-P metamorphism (e.g., Spear and Cheney 1989; Powell and Holland 1990; Xu et al. 1994), and also for partial melting processes (White et al. 2000, 2001). However, a petrogenetic grid for high-P metapelites has not been presented.

Since the 1970s, the unusual pelitic assemblages such as kyanite–talc, phengite–talc and pyrope–coesite, with the former two being called whiteschists by Schreyer (1977), have been reported from a number of districts of the world (Vrana and Barr 1972; Kulke and Schreyer 1973; Abraham and Schreyer 1976; Chopin 1981, 1984; Izadyar et al. 2000). These finds stimulated the experimental study of the stability of these unusual assemblages, and of the variations of mineral composition such as the Si contents in phengite with respect to pressure and temperature in the MASH and KMASH systems (Schreyer 1977; Chopin and Schreyer 1983; Chopin 1986; Massonne and Schreyer 1987; Schreyer 1988; Massonne 1989; Massonne and Schreyer 1989; Massonne and Szpurka 1997). Actually, the natural parageneses of talc–kyanite and talc–phengite usually coexist with chloritoid, garnet, biotite and chlorite, etc. which, in most cases, contain considerable amounts of Fe and do not belong to the constituents of the simple MASH and KMASH systems. For example, the phengite–talc paragenesis described by Chopin (1981)

from the Western Alps includes mineral assemblages chloritoid + phengite + talc + quartz, chloritoid + phengite + talc + chlorite + quartz, chloritoid + phengite + talc + garnet + quartz, and chloritoid + talc + kyanite + phengite + quartz (excluding those with Na-bearing phases), and the paragenesis talc–kyanite occurring together with garnet, phengite and quartz has been reported from Tasmania (Råheim and Green 1974), northern Kazakhstan (Udovkina et al. 1977) and the Eastern Alps (Frank et al. 1987). Moreover, other pelitic assemblages have been described from different high-*P* terranes, such as garnet–kyanite–phengite quartzite from the Central Alps (Meyre et al. 1999), carpholite- and chloritoid-bearing metapelites from Crete and the Peloponnese, Greece (Theye et al. 1992), paragneisses composed mainly of garnet, phengite, biotite and quartz from the Dabie ultrahigh-*P* terranes, Central China (Wang and Liou 1991; Liou et al. 1995), and so on. At present, the phase relations and *P–T* conditions of these high-*P* assemblages have not been well delineated. Furthermore, the pressure estimation of these assemblages, in many cases, has to rely on the phengite geobarometers which were experimentally calibrated in the limited KMASH assemblages talc–kyanite–quartz–phengite (tks-phengite) and talc–phlogopite–quartz–phengite (tps-phengite; Massonne and Schreyer 1989; Massonne and Szpurka 1997). It needs to be established whether these phengite geobarometers can be used on natural rocks with mineral assemblages deviating from these limited KMASH assemblages.

In this paper, petrogenetic grids in the model system KFMASH and the subsystems KMASH and KFASH have been calculated in the *P–T* range 5–36 kbar and 400–810 °C, using THERMOCALC 3.1 (Powell et al. 1998) and the internally consistent thermodynamic dataset of Holland and Powell (1998) as well as updated models of activity–composition relationships (details presented in the Appendix) for the minerals garnet, chloritoid, biotite, carpholite, talc, chlorite, staurolite and kyanite/sillimanite with phengite, quartz/coesite and H_2O in excess. As mentioned above, all these minerals are commonly reported from high-*P* metapelites around the world. Other high-*P* phases such as sudoite are extensive in high-*P* and low-*T* metapelites (Schreyer 1988; Theye et al. 1992). However, it is ruled out in this study because, according to Fransolet and Schreyer (1984), its upper thermal limit is about 380 °C, out of the temperature range of our interest. The calculated grids, together with the calculated AFM compatibility diagrams and *P–T*, *T–X* and *P–X* pseudosections for various bulk compositions, are employed to decipher the phase equilibria and *P–T* conditions of natural metapelites from different high-*P* terranes. Moreover, the phengite Si isopleths contoured in a series of *P–T* pseudosections are used to estimate the equilibrium pressures for various natural assemblages, and to provide a brief evaluation of the current phengite geobarometers.

Petrogenetic grids

The calculated *P–T* projections in the KMASH, KFASH and KFMASH systems are presented in Figs. 1 and 2, and information on the invariant points is tabulated in Table 1.

KMASH grid

In the KMASH grid (Fig. 1a), only two invariant points are stable in the *P–T* range of interest involving the phases biotite, chlorite, talc, carpholite and kyanite

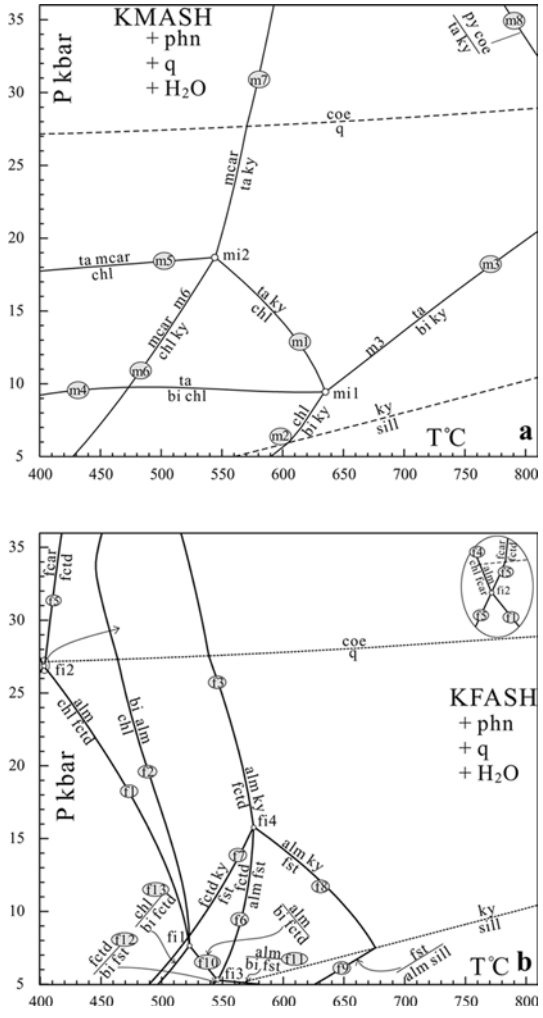

Fig. 1a, b *P–T* projections for the subsystem KMASH (**a**) and KFASH (**b**) in projection from phengite, quartz and H_2O. Labels *m1–m8* and *mi1–mi2* refer to the univariant reactions and invariant points in the KMASH system, respectively, and labels *fi1–fi4* and *f1–f13* to the invariant points and univariant reactions in the KFASH system, respectively. The reactions coe = q and ky = sill are shown as *thick dashed lines*. Mineral abbreviations: *alm* almandine, *bi* biotite, *chl* chlorite, *coe* coesite, *fcar* Fe-carpholite, *fctd* Fe-chloritoid, *fst* Fe-staurolite, *ky* kyanite, *mcar* Mg-carpholite, *q* quartz, *ta* talc, *phn* phengite, *py* pyrope, *sill* sillimanite

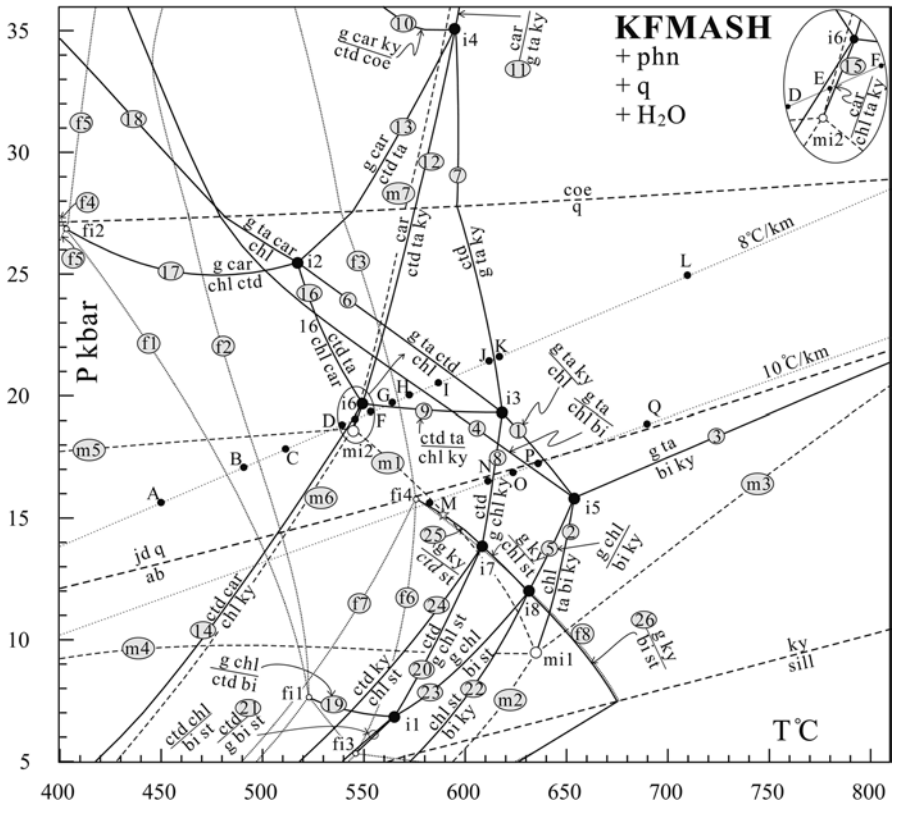

Fig. 2 *P–T* projection for the full system KFMASH in projection from phengite, quartz and H_2O. Labels *i1–i8* and *1–26* are the invariant points and univariant reactions in the KFMASH system discussed in the text. Full system reactions terminating at subsystem invariant points are shown by *large* and *small open circles*, respectively. The subsystem reactions in the KMASH are shown as the *dashed lines* with labels *m1–m7*, and the reactions in the KFASH as the *dotted lines* with labels *f1–f8*. The *open star* indicates the location of singularity, and the phases which 'swap' sides of the reaction are shown in *italics*. The reactions coe = q, jd + q = ab and ky = sill are shown as *thick dashed lines*. *A–Q* are the locations of the AFM compatibility diagrams shown in Figs. 3 and 4. Mineral abbreviations: *ab* albite, *car* carpholite, *ctd* chloritoid, *g* garnet, *jd* jadeite, *st* staurolite; for others, see Fig. 1

(+ phengite, quartz, H_2O). The characteristic paragenesis for whiteschist talc–kyanite (Schreyer 1977) occupies a wide field bounded by reactions m1 (chl + q = ta + ky), m3 (ta + phn = bi + ky) and m7 (mcar = ta + ky) on the lower *P–T* sides, and will break down to form pyrope and coesite at very high *P* and *T* via reaction m8 (ta + ky = py + coe). This reaction, experimentally studied by Chopin (1986), is of great interest as it was undoubtedly instrumental in the formation of the small pyrope crystals containing relics of coesite in the sugary pyrope quartzite studied by Chopin (1984) from the Dora Maira Massif. The paragenesis talc–phengite confined by reactions m4 (bi + chl = ta + phn) and m3 takes up a wider field than does talc–kyanite.

In the presence of quartz and phengite, reactions m1, m2 and m5 define the maximum stability of chlorite, and reactions m6 and m7 limit the stability of Mg-carpholite.

There are no stable invariant points and univariant reactions involving Mg-chloritoid and Mg-staurolite. This is in agreement with the previous conclusion that there is no compatibility of Mg-chloritoid and Mg-staurolite with a SiO_2 phase (Schreyer 1988).

KFASH grid

The calculated *P–T* projection in the KFASH subsystem is displayed in Fig. 1b which includes four stable invariant points involving the mineral phases biotite, chlorite, almandine, Fe-chloritoid, Fe-carpholite and Fe-staurolite with phengite, quartz/coesite and H_2O in excess. Univariant curves emanating from these invariant points define the maximum stability fields of some of the Fe-end members. For example, reactions f1 (chl + fctd = alm), f4 (chl + fcar = alm), f10 (bi + fctd = alm) and f11 (bi + fst = alm) demarcate the low-*T* and/or low-*P* limit of almandine. Reactions f3 (fctd = alm + ky), f6 (fctd = alm + fst) and f12 (fctd = bi + fst) restrict the high-*T* limit of Fe-chloritoid, and reaction f5 (fcar = fctd) restricts its low-*T* limit. The stability of Fe-staurolite is confined by reactions f7 (fctd + ky = fst), f8 (fst = alm + ky) and f9 (fst = alm + sill), stable at pressures lower than 15.82 kbar (fi4). If phengite is in excess, reactions f2 (chl + phn = bi + alm) and f13 (chl + phn = bi + fctd) confine the high-*T* limit of Fe-chlorite. Unlike the KMASH subsystem, there are no Fe-talc-related reactions stable in the *P–T* range of interest in the KFASH.

KFMASH grid

The full system KFMASH grid together with the subsystem KMASH and KFASH equilibria are shown in Fig. 2. There are eight full system invariant points stable in the *P–T* range of interest, which are denoted by large closed circles, and the KMASH and KFASH subsystem invariant points are denoted by large and small open circles.

In the KFMASH system, the stability of carpholite, confined by reactions 14, 15, 12 and 11, is almost the same as that in KMASH. With the presence of quartz/coesite and phengite, the maximum stability of

Table 1 Calculated results for stable invariant equilibria in the systems KMASH, KFASH and KFMASH, with uncertainties of P–T conditions

Equilibrium	P (kbar)	SD (P)	T (°C)	SD (T)	x(g)[a]	x(ctd)	x(phn)	y(phn)	x(bi)	y(bi)	Q(bi)	x(chl)	y(chl)	N(chl)	x(car)	x(ta)	y(ta)	x(st)
KMASH																		
Equil. mi1: bi, chl, ta, ky, (phn, q, H_2O)	9.43	0.7	635.1	6				0.861		0.347			0.546	0.455			0.092	
Equil. mi2: chl, ta, mcar, ky, (phn, q, H_2O)	18.68	0.5	544.4	4				0.729					0.519	0.481			0.041	
KFASH																		
Equil. fi1: bi, chl, alm, fctd, (phn, q, H_2O)	7.65	1.6	522.7	11				0.874		0.487			0.545	0.455				
Equil. fi2: chl, alm, fctd, fcar, (phn, q, H_2O)	26.88	1.2	402.8	10				0.284					0.501	0.499				
Equil. fi3: bi, alm, fctd, fst, (phn, q, H_2O)	5.27	0.9	546.0	7				0.938		0.685								
Equil. fi4: alm, fctd, ky, fst, (phn, q, H_2O)	15.82	0.7	575.5	5				0.861										
KFMASH																		
Equil. i1: g, ctd, chl, bi, st, (phn, q, H_2O)	6.85	1.5	565.1	15	0.935	0.860	0.665	0.907	0.759	0.521	0.123	0.677	0.606	0.394				0.937
Equil.i2: g, ctd, chl, car, ta, (phn, q, H_2O)	25.47	0.7	517.2	11	0.834	0.622	0.332	0.427				0.384	0.505	0.495	0.232	0.100	0.016	
Equil. i3: g, ctd, chl, ta, ky, (phn, q, H_2O)	19.32	0.9	618.3	6	0.638	0.417	0.225	0.679				0.224	0.524	0.476		0.070	0.051	
Equil.i4: g, ctd, car, ta, ky, (phn, coe, H_2O)	35.15	3.1	595.4	5	0.523	0.276	0.132	0.426							0.083	0.032	0.020	
Equil. i5: g, chl, bi, ta, ky, (phn, q, H_2O)	15.83	0.5	653.7	6	0.588		0.216	0.737	0.240	0.162	0.382	0.203	0.533	0.467		0.071	0.068	
Equil.i6: ctd, chl, car, ta, ky, (phn, q, H_2O)	19.67	0.7	549.3	6		0.133	0.055	0.703				0.059	0.518	0.481	0.033	0.014	0.039	
Equil.i7: g, ctd, chl, st, ky, (phn, q, H_2O)	13.85	0.6	608.4	5	0.777	0.594	0.359	0.800				0.356	0.546	0.454				0.787
Equil. i8: g, chl, bi, st, ky, (phn, q, H_2O)	11.96	0.6	631.1	6	0.736		0.332	0.821	0.356	0.240	0.416	0.318	0.552	0.448				0.756

[a] $x(g) = Fe/(Mg+Fe)$, $x(ctd) = Fe/(Mg+Fe)$, $x(car) = Fe/(Fe+Mg)$, $x(chl) = Fe/(Fe+Mg)$, $y(chl) = x_{Al}^{T2} = Al/4$, $N(chl) = (x_{Al}^{M4} - x_{Al}^{M1})/2$, $x(phn) = Fe/(Fe+Mg)$, $y(phn) = x_{Al}^{M2A}$, $x(bi) = Fe/(Fe+Mg)$, $y(bi) = x_{Al}^{M1}$, $Q(bi) = x_{Fe}^{M1} - x_{Fe}^{M2}$, $x(ta) = Fe/(Fe+Mg)$, $y(ta) = x_{Al}^{M3}$, $x(st) = Fe/(Mg+Fe)$

KFMASH chlorite is much larger than those of Mg- and Fe-chlorite in the subsystems. At pressures below i3, chlorite is confined by reactions 1 (chl = g + ta + ky) and 2 (chl + phn = ta + bi + ky), stable at higher temperatures than chloritoid, but at pressures above i3, chlorite is limited by reactions 6 (chl = g + ta + ctd) and 18 (chl = g + ta + car), stable at lower temperatures than chloritoid. With the presence of quartz/coesite and, at lower pressures, of phengite, chloritoid breaks down via reactions 21 (ctd + phn = g + bi + st), 20 (ctd = g + chl + st), 8 (ctd = g + chl + ky), 7 (ctd = g + ta + ky) and 10 (ctd = g + car + ky) which, for pressure ranges between invariant points i1 and i4, are vertically sloped and can be used as good temperature indicators.

The whiteschist parageneses talc–kyanite and talc–phengite, in the KFMASH, are always associated with combinations of chlorite, chloritoid and garnet, reducing their stability fields to higher pressures (see below).

Guiraud et al. (1990) calculated a NFMASH grid for the greenschist–blueschist–eclogite facies in the range 5–50 kbar and 300–850 °C. Of the 18 NFMASH invariant points presented in their grid, three of them correspond to i3, i6 and i2 in Fig. 2, with distinctly different *P–T* conditions of 23.3 kbar at 631 °C, 28 kbar at 584 °C, and 43 kbar at 589 °C, respectively, which in turn leads to a considerable difference in the phase topologies between the two grids. These differences arise from the substantial improvements in the internally–consistent dataset and activity–composition models for the solid solutions since 1990. As mentioned above and below, the present calculations are in good agreement with the petrological observations.

Compatibility diagrams

To illustrate the changes in mineral assemblage and mineral composition with respect to *P–T* and bulk composition, a series of calculated AFM compatibility diagrams with phengite, quartz and H_2O in excess were drawn for a traverse approximately along a geotherm 8 °C/km from locations A–L in Fig. 2 and presented in Fig. 3.

In Fig. 3, location A, the ctd–car tie line is stable. Appropriate bulk compositions which projected between the ctd–car tie line and chlorite give the common assemblages such as ctd + car + chl, ctd + chl and car + chl, etc., in western Crete and the Peloponnese, Greece (Theye et al. 1992). If the bulk composition is more aluminous, kyanite will coexist with chloritoid and/or carpholite, but not chlorite. The KMASH subsystem reaction m4 (bi + chl = ta + phn) becomes continuous in the full system, giving the chl–ta–bi divariant triangle in Mg- and K-rich rocks. At this stage, both chlorite and biotite are complete solid solutions between Fe- and Mg-end members. When the KFASH reaction f1 (chl + fctd = alm) is crossed, almandine-rich garnet appears in Fe-rich rocks, producing the g–ctd–chl divariant triangle in Fig. 3, location B. As *P–T* increases to meet

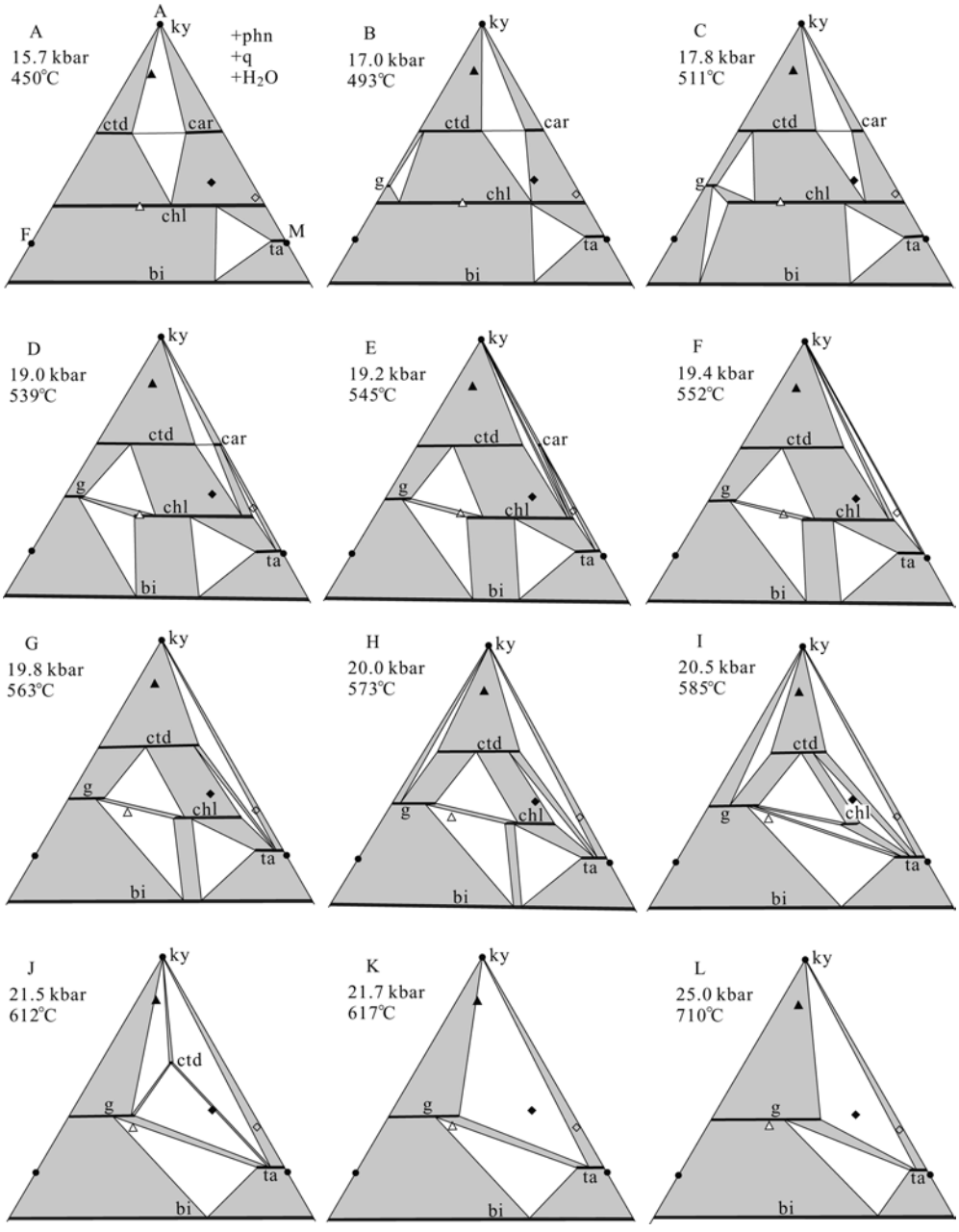

Fig. 3 AFM compatibility diagrams in projection from phengite, quartz and H_2O calculated for the locations *A–L* labeled in Fig. 2, and their *P–T* conditions. The *open diamond*, *closed diamond*, *closed triangle* and *open triangle* represent the projections of bulk composition of samples a42, 7-37, CHM39 and M4, respectively, discussed below

the subsystem reaction f2 (chl + phn = alm + bi), Fe-chlorite breaks down and garnet starts coexisting with biotite (Fig. 3, location C). As shown in Fig. 3, location D, the subsystem reaction m5 (chl = mcar + ta) results in the decomposition of Mg-chlorite and the divariant triangle chl–car–ta. From locations A to D, the ctd–car tie line has been available and both minerals become richer in Mg as *P–T* increases. This tie line is broken by the full system reaction 14 (ctd + car = chl + ky), giving rise to the chl–ky tie line in Fig. 3, location E. The KMASH reaction m7 (car = ta + ky) and KFMASH reaction 15 (car = chl + ta + ky) result in the decomposition of carpholite and the appearance of the typical whiteschist assemblage ta–ky in Mg-rich rocks (Fig. 3, location F). Across reaction 9 (chl + ky = ctd + ta), the chl–ky tie line gives its way to ctd–ta in Fig. 3, location G which, as shown by its flat slope in Fig. 2, is a good pressure indicator. Next, the subsystem reaction f3 (fctd = alm + ky) leads to the breakdown of Fe-chloritoid and the appearance of the divariant triangle g–ctd–ky in Fig. 3, location H. Garnet starts to coexist with talc through reaction 4 (chl + bi = g + ta + phn), first occurring in Al-poor and K-rich rocks (Fig. 3, location I). Across reaction 6 (chl = g + ctd + ta), chlorite disappears from the system (Fig. 3, location J). At this stage, the surviving chloritoid shows a narrow composition range. Finally, the KFMASH reaction 7 leads to the disappearance of chloritoid and the appearance of g + ta + ky (Fig. 3, location K). With further *P–T* increase, the phase topology does not change, although the three solid

solutions garnet, biotite and talc become more Mg-rich (Fig. 3, location L).

For a geotherm of 10 °C/km and from locations M to Q in Fig. 2, the changes in mineral topology are shown in Fig. 4. In Fig. 4, location M, the chl–ky tie line is available and carpholite would have disappeared in virtue of the full system reaction 14 (car + ctd = chl + ky) and the subsystem reaction m6 (mcar = chl + ky) in Al- and Mg-rich rocks. The KMASH reaction m4 (chl + bi = ta) produces the divariant triangle chl–bi–ta in Mg- and K-rich rocks. In Fe- and Al-rich rocks, the KFMASH reaction 25 (st = g + ctd + ky, above the singularity) results in the coexistence of g–ctd–ky and the breakdown of staurolite in the system. The subsystem reaction f1 (chl + fctd = alm) leads to the divariant triangle g–ct–chl in Al-richer rocks, and f2 (chl + phn = alm + bi) to the triangle g–chl–bi in K-richer rocks. With *P–T* increasing, the KMASH reaction m1 (chl = ta + ky) causes the disappearance of Mg-chlorite and the coexistence of talc and kyanite in Mg-rich rocks (Fig. 4, location N). At this stage, the chloritoid shows a narrow composition range which is clearly more Fe-rich than that in location J at higher pressure and almost the same temperature. As shown in Fig. 4, location O, this survived chloritoid is broken down through reaction 8. As for *P–T* crossing reaction 4, the g–ta coexistence appears in Al-poor and K-rich rocks (Fig. 4, location P). Finally, chlorite breaks down to produce the assemblage g + ta + ky via reaction 1. Unlike the process at higher *P*, chloritoid breaks down before chlorite, and there is no coexistence of chloritoid and talc in this metamorphic process.

For comparison, four bulk compositions which will be discussed below are projected on each AFM diagram of Figs. 3 and 4.

Applications

Application of the KMASH grid

Schreyer (1977) reported several bulk compositions for typical whiteschist in which a representative sample (a42) is selected for discussion here. The sample a42 contains SiO_2 56.20, Al_2O_3 16.00, MgO 22.90 and K_2O 0.20 (wt%), giving Al_2O_3:MgO:K_2O = 21.58:78.13:0.29 on a mole basis. Using this bulk composition, a *P–T* pseudosection of the KMASH grid (Fig. 1a) is calculated and presented in Fig. 5a. It is dominated by divariant fields with only one, small trivariant field in the lower-left corner. The characteristic assemblage of whiteschist ky + ta takes up a large *P–T* range bounded by reactions m1, m3, m7 and m8. For this specific bulk composition, there is insufficient K_2O to have phengite once biotite becomes stable. Hence, the phengite-absent reaction chl = ta + ky/sill becomes stable and is shown in Fig. 5a with a label m1′. The calculated isopleths of Si content in phengite in the phengite-bearing fields in Fig. 5a show a systematic increase of Si with pressure. Moreover, the isopleths in the divariant field ta + ky + phn approximate closely the ones determined experimentally by Massonne and Schreyer (1989), except that the isopleths with lower Si content show slightly negative slopes. However, the isopleths with Si < 3.30 were not well constrained in the experiments of Massonne and Schreyer (1989). This gives a possibility for Fig. 5a to be a geobarometer not only for rocks with the experimentally studied limiting assemblage kyanite + talc + phengite but also for rocks with other assemblages. It should be pointed out that the phengite Si isopleths are strongly dependent on mineral assemblages

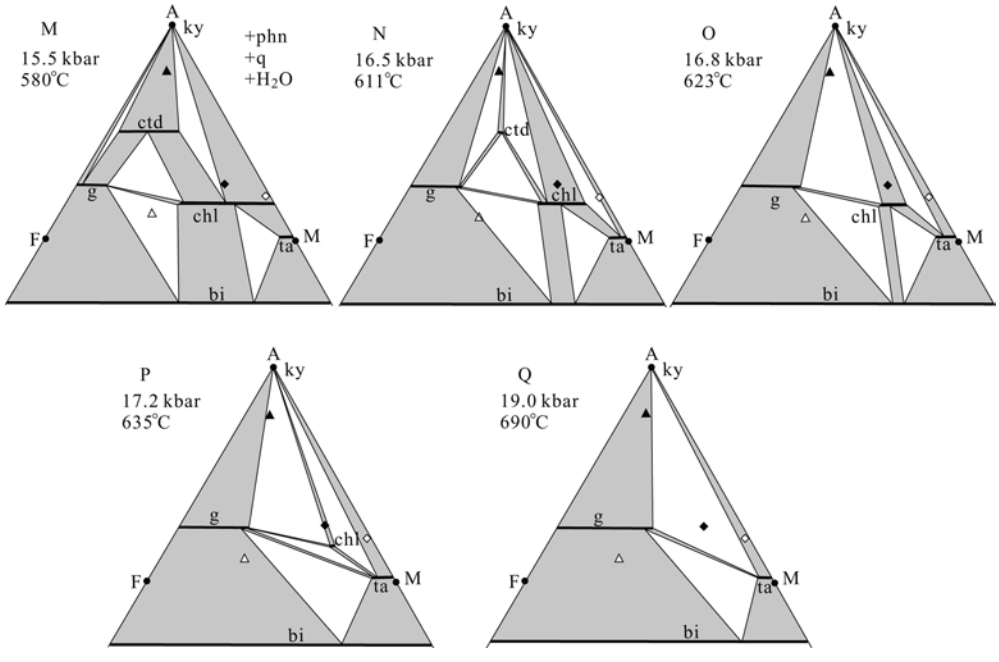

Fig. 4 AFM compatibility diagrams in projection from phengite, quartz and H_2O calculated for the locations *M–Q* labeled in Fig. 2, and their *P–T* conditions (for other information, see Fig. 3)

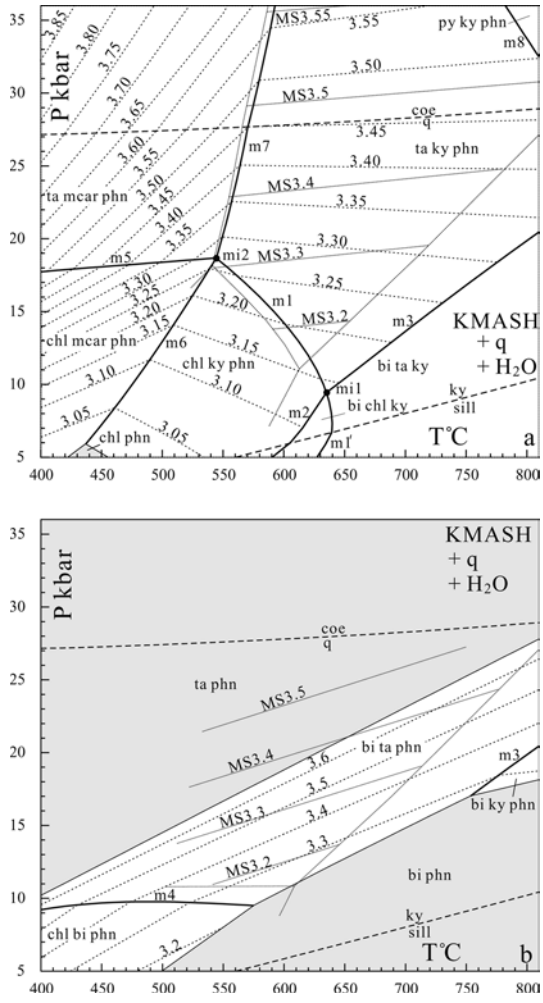

Fig. 5 a *P–T* pseudosection in the KMASH subsystem, with quartz and H_2O in excess, for the typical whiteschist of Schreyer (1977), sample a42, with Al_2O_3:MgO:K_2O = 21.58:78.13:0.29, showing the invariant points (*closed circles*) and univariant reactions (*thick solid lines*) with labels the same as in Fig. 1 encountered by the bulk composition, divariant fields (*unshaded*) and trivariant fields (*lighter-shaded*). For this particular bulk composition, phengite is not in excess and the phengite-absent reaction chl = ta + ky is encountered and labeled as m1′, separating the divariant fields bi–chl–ky/sill and bi–ta–ky/sill. Isopleths of the Si contents in phengite are contoured as *dashed lines* with values (Si =)3.05–3.85 p.f.u. For comparison, the phengite Si isopleths deduced by Massonne and Schreyer (1989) from their experiments are denoted as *thick dashed lines* with labels *MS3.2–MS3.55*. **b** *P–T* pseudosection in the KMASH subsystem, with phengite, quartz and H_2O in excess, for an experimental gel (number 11) used by Massonne and Schreyer (1989) with Al_2O_3:MgO:K_2O = 24.46:61.05:14.49, showing the univariant reactions (*thick solid lines* with labels the same as Fig. 1) encountered by the bulk composition, divariant fields (*unshaded*) and trivariant fields (*lighter-shaded*). Isopleths of the Si content in phengite are shown as the *dashed lines* with values (Si =)3.2–3.6 p.f.u. For comparison, the phengite Si isopleths experimentally determined by Massonne and Schreyer (1989) are denoted as *thick dashed lines* with labels *MS3.2–MS3.5*

with which phengite occurs. For example, in the field ta + mcar + phn in Fig. 5a, the Si isopleths are markedly different in slope and contour interval from those shown for the ta + ky + phn field.

Massonne and Schreyer (1989) also experimentally calibrated the stability of the assemblage talc–phengite–phlogopite–quartz using four gels (numbers 8–11) which are poor in Al_2O_3 and rich in K_2O. As an example, we selected the K_2O-richest gel 11 to calculate its *P–T* pseudosection. This gel contains SiO_2 62.8, Al_2O_3 14.7, MgO 14.5 and K_2O 8.05 (wt%), giving Al_2O_3:MgO:K_2O = 24.46:61.05:14.49 on a mole basis. The calculated *P–T* pseudosection is presented in Fig. 5b. There are three divariant fields chl + bi + phn, ta + bi + phn and bi + ky + phn which are sandwiched between two trivariant fields ta + phn and bi + phn. When the divariant fields are contoured for the phengite Si contents, it shows that the Si contents rise linearly with pressure which, however, matches poorly the experimentally calibrated curves of Massonne and Schreyer (1989). As depicted by Massonne and Schreyer (1989), the experimentally calibrated tps-phengite barometer turned out to be of inferior quality, probably because the experimental phengites contained higher octahedral occupancies which would lead to an underestimation of Si contents. Massonne and Schreyer (1989) presented two examples to test their tps-phengite barometer. One is the garnet–piemontite schist described by Abraham and Schreyer (1976) from Serbia in which the phengite coexists with Ca- and Mn-rich garnet, chlorite, phlogopite and talc, and the maximum Si content of 3.29 yields a metamorphic pressure of 13 kbar for a temperature of 500 °C with their tps-phengite geobarometer. The other is the metapelite from the Gran Paradiso Massif where, as shown by sample 6-255 (Chopin 1981) and cited by Massonne and Schreyer (1989), the phengite coexisting with talc, phlogopite, chlorite, garnet, quartz and hematite contains the Si content of 3.55, indicating a metamorphic pressures of 23 kbar for an estimated temperature of 500 °C based on their tps-phengite geobarometer. This estimation, as discussed by Massonne and Schreyer (1989), is in contrast to the metamorphic pressures of only 14–15 kbar deduced by Massonne and Chopin (1989) for the adjacent metagranites.

Strictly speaking, both the above examples deviate from the KMASH-limiting assemblage. The garnet–piemontite schist presented in the first example contains considerable amounts of manganese in its bulk composition which could not be well delineated by the model KMASH and even the KFMASH system. The phengite with Si = 3.55 in the second example provides a metamorphic pressure of 13 kbar for an estimated *T* = 500 °C according to Fig. 5b, which is quite close to the result of 14–15 kbar for the adjacent metagranites, supporting the calculated phengite Si isopleths.

Application of the KFMASH grid

Three types of pelitic assemblages from different high-*P*/*T* metamorphic terranes are selected to apply the KFMASH grid.

Talc–phengite high-grade pelitic blueschists of the Western Alps

Chopin (1981) reported that the assemblage ta–phn is widespread in the high-grade pelitic blueschist facies rocks in and around the Gran Paradiso Massif of the Western Alps. The rocks are essentially composed of talc, phengite, chloritoid and quartz (±chlorite, ±garnet), with minor Na-bearing minerals in some samples. For example, one representative sample 7-37, with an assemblage ctd + ta + chl + phn + q, has a bulk composition with SiO_2 43.71, Al_2O_3 24.17, FeO 7.08, MgO 14.67 and K_2O 2.64 (wt%), giving Al_2O_3:MgO:FeO:-K_2O = 32.57:50.03:13.54:3.85 on a mole basis. Using this bulk composition, a calculated *P–T* pseudosection is presented in Fig. 6, which is dominated by di- and trivariant fields with only a small quadrivariant variant field and four invariant points which can be seen in this bulk composition. Contouring of the phengite Si isopleths in the phengite-bearing fields indicates that the Si contents rise linearly with pressure. The mineral assemblage corresponding to that observed in sample 7-37, ctd + ta + chl + phn, takes up a narrow strip in the center of Fig. 6, indicating a *P–T* range of 19–22 kbar and 530–620 °C. The phengite in this mineral assemblage has Si = ~3.4, which is in good accord with the calculated Si value, giving a more specific *P–T* range for the rock of 22.5 kbar and 540–570 °C.

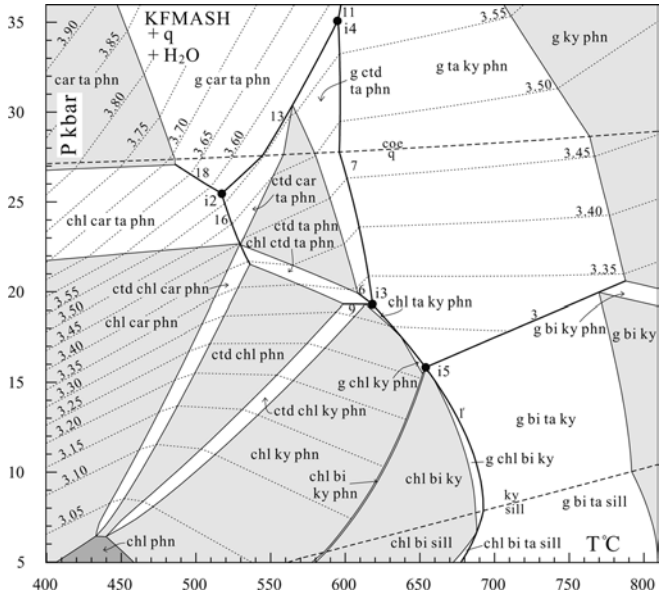

Fig. 6 *P–T* pseudosection in the KFMASH system, with quartz and H_2O in excess, for a chloritoid–talc–phengite schist (sample 7-37) from the Western Alps (Chopin 1981) with Al_2O_3:MgO:FeO:-K_2O = 32.57:50.03:13.54:3.85, showing the invariant points (*closed circles*) and univariant reactions (*thick solid lines*) encountered by the bulk composition, divariant fields (*unshaded*), trivariant fields (*lighter-shaded*) and quadrivariant fields (*darker-shaded*). The labels are as for Fig. 2. Isopleths of the Si content in phengite are shown as *dashed lines* with values (Si =)3.05–3.90 p.f.u. For this bulk composition, phengite is not in excess when biotite appears, and the phengite-absent reaction chl = g + ta + ky is encountered and displayed with a label 1′

Figure 7a and b are the T–X_{Mg} and P–X_{Mg} pseudosections for sample 7-37 drawn at P = 21 kbar and T = 580 °C, respectively, which indicate the mineral assemblages with respect to changes in temperature, pressure and X_{Mg}. These pseudosections contain only di- and trivariant fields. The subsystem reactions f1, f3, f8, m1 and m7 encountered by this bulk composition become continuous in the full system, and are displayed as reaction loops cut by the full system reactions. Figure 7b also shows isopleths of the phengite Si content which rises linearly with pressure, and changes with X_{Mg} within trivariant fields but does not change with X_{Mg} within divariant fields. The observed assemblage ctd + ta + chl + phn + q for sample 7-37 takes up a small field

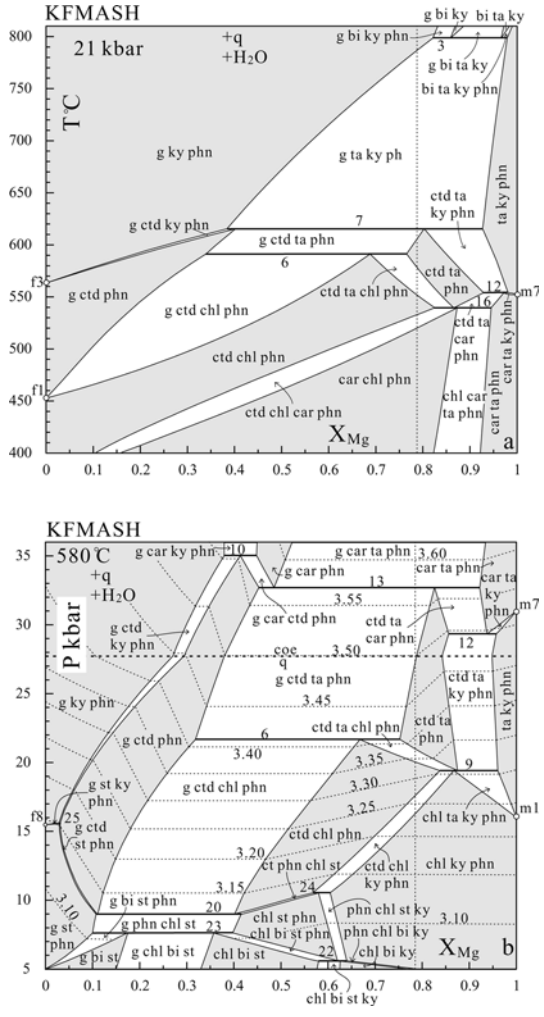

Fig. 7a, b T–X_{Mg} (**a**) and P–X_{Mg} (**b**) pseudosections at 21 kbar and 580 °C, respectively, in the KFMASH system with quartz and H_2O in excess for sample 7-37, showing the univariant reactions (*thick solid lines*) with labels the same as in Fig. 2 encountered by the bulk composition, divariant fields (*unshaded*) and trivariant fields (*lighter-shaded*). Subsystem reactions are denoted as *small open circles*, with labels the same as in Figs. 1 and 2. Isopleths of the phengite Si content are shown as the *dashed lines* with values (Si =)3.10–3.60 p.f.u. in **b**. The *vertical dashed line* in each diagram shows the X_{Mg} (= MgO/(MgO + FeO)) value for the bulk composition of sample 7-37

which is confined, in temperature, by reactions 16 and 6 in Fig. 7a and, in pressure, by reactions 9 and 6 in Fig. 7b. The line with $X_{Mg} = 0.78$ is the actual X_{Mg} for sample 7-37. If the bulk composition is richer in Mg, the mineral assemblages from both Fig. 7a and b would be ctd + ta + phn and ctd + ta + ky + phn and, if the bulk composition is poorer in Mg and/or P/T is higher (above reaction 6), garnet would coexist with chloritoid, talc and phengite. All of these are the mineral assemblages described by Chopin (1981) from the Gran Paradiso and Monte Rosa massifs of the Western Alps.

High-P metapelites from the Central Alps

Meyre et al. (1999) described the Tertiary high-*P* metapelites from the Adula Nappe, Central Alps, Switzerland, which are generally composed of garnet, phengite, kyanite, quartz and/or paragonite. A representative sample (CHM39) contains phengite (10%) + garnet (20%) + kyanite (20%) + quartz (50%). Using these mineral modal proportions and their microprobe analyses listed in Meyre et al. (1999), an effective bulk composition (Vance and Holland 1993) is generated with THERMOCALC, giving Al_2O_3:MgO:FeO:K_2O = 76.63:8.82:12.01:2.55 on a mole basis. Using this bulk composition, a *P–T* pseudosection calculated for sample CHM39 is presented in Fig. 8. It is characterized by the prevalence of di- and trivariant fields with three invariant points which can be seen in this bulk composition. The *P–T* pseudosection is also contoured by the phengite Si isopleths which are negatively sloped at temperatures below 600–650 °C, and positively sloped at higher temperatures. The observed assemblage g + ky + phn + q for sample CHM39 is trivariant and stable over a wide *P–T* range, with pressures above 13 kbar and temperatures over ca. 600 °C. The phengite in sample CHM39 has Si = 3.4 p.f.u. which provides a pressure range of about 23.5–26 kbar for the temperatures ranging from 600 °C (should be over 620 °C from Fig. 8) to 700 °C estimated by Meyre et al. (1999). This value is in agreement with the peak pressure condition of 25 kbar suggested by Meyre et al. (1999) from the associated sodic whiteschist samples in the Adula Nappe, where peak pressures for the Na-poor metapelites like CHM39 were not well constrained.

Figure 9a, b show the T–X_{Mg} and P–X_{Mg} pseudosections for sample CHM39 calculated at $P = 21$ kbar and $T = 580$ °C, respectively, which indicate clearly the changes of mineral assemblage with respect to pressure, temperature and X_{Mg}. The subsystem reactions f3 and m7 in Fig. 9a, and f8, m1 and m7 in Fig. 9b become continuous in the full system and are displayed as reaction loops truncated by the full system reactions. Contours of the phengite Si content in Fig. 9b rise linearly with pressure, decrease with X_{Mg} in the trivariant fields g–ky–phn, st–ky–phn and ctd–ky–phn with relatively lower X_{Mg}, but increase with X_{Mg} in the trivariant fields car–ky–phn and ta–ky–phn with higher X_{Mg}. In all

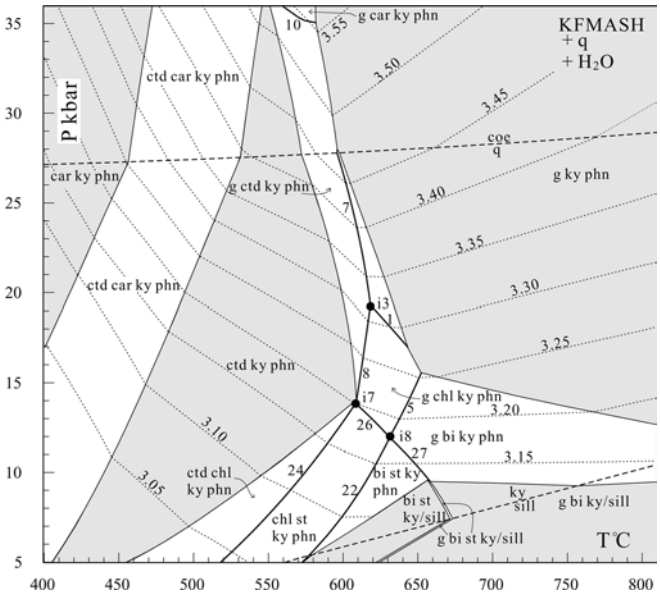

Fig. 8 *P–T* pseudosection in the KFMASH, with quartz and H_2O in excess, for a garnet–kyanite–phengite schist (sample CHM39) from the Central Alps (Meyre et al. 1999) with Al_2O_3:MgO:FeO:K_2O = 76.63:8.82:12.01:2.55, showing the invariant points (*closed circles*) and univariant reactions (*thick solid lines*) with labels the same as in Fig. 2 encountered by the bulk composition, divariant fields (*unshaded*) and trivariant fields (*lighter-shaded*). Isopleths of the Si content in phengite are shown as the *dashed lines* with values (Si =)3.05–3.55 p.f.u.

the divariant fields, the phengite Si isopleths do not vary with X_{Mg}.

Compared with the bulk composition of sample 7-37, sample CHM39 is much more aluminous and poorer in Mg. So, kyanite is present in almost every di- and trivariant mineral assemblage in Figs. 8 and 9a, b, no matter what P, T and X_{Mg} values are.

Paragneisses from the Dabie ultrahigh-P terranes, Central China

The regional ultrahigh-*P* metamorphism in the Dabie Mountains, Central China is well known mainly from investigations on eclogite, especially on diamond- and coesite-bearing eclogite blocks. Whether the extensively distributed paragneisses hosting these eclogite blocks have been subjected to the ultrahigh- and/or high-*P* metamorphism is still controversial because of the lack of available geobarometers, although some ultrahigh-*P* relics have been reported from these rocks (Wang and Liou 1991; Liu et al. 2001). These paragneises are generally composed of garnet, phengitic muscovite, biotite, quartz, plagioclase, epidote, rutile and ilmenite. For example, a representative sample (M4) for these paragneisses described by Wei et al. (1996, unpublished data) is composed of garnet (15) + biotite (15) + phengite (18) + quartz (40) + plagioclase (10 vol%) and small amounts of rutile and magnetite. The microprobe analyses for the main minerals are, for garnet SiO_2 37.53,

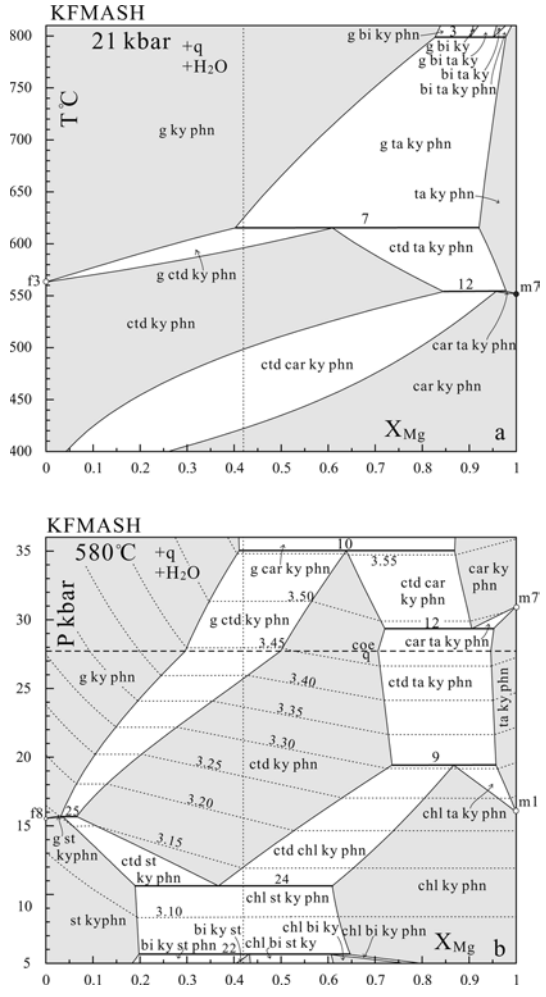

Fig. 9a, b T–X_{Mg} (**a**) and P–X_{Mg} (**b**) pseudosections at 21 kbar and 580 °C, respectively, in the KFMASH system, with quartz and H_2O in excess for sample CHM39, showing the univariant reactions (*thick solid lines*) with labels the same as in Fig. 2 encountered by the bulk composition, divariant fields (*unshaded*) and trivariant fields (*lighter-shaded*). Subsystem reactions are denoted as *small open circles* and with labels the same as in Fig. 1. Isopleths of the phengite Si content are shown as *dashed lines* with values (Si =)3.10–3.55 p.f.u. in **b**. The *vertical dashed line* in each diagram shows the X_{Mg} (= MgO/(MgO + FeO)) value for the bulk composition of sample CHM39

Al_2O_3 21.32, FeO 26.75, MgO 6.28, and CaO 5.67 (wt%), for phengite SiO_2 49.40, Al_2O_3 28.94, FeO 2.37, MgO 2.89, and K_2O 11.54 (wt%), and for biotite SiO_2 36.55, Al_2O_3 18.36, FeO 16.87, MgO 10.87, and K_2O 10.52 (wt%). Neglecting the presence of a small amount of plagioclase and CaO in garnet, an effective bulk composition for sample M4 can be generated in the KFMASH system with THERMOCALC from the above mineral modal proportions and compositions, giving Al_2O_3:MgO:FeO:K_2O = 34.29:23.32:29.97:12.41 on a mole basis. Using this bulk composition, a P–T pseudosection was calculated for sample M4 and is presented in Fig. 10. This pseudosection includes di-, tri- and quadrivariant fields with only one invariant point i2 which can be seen in this bulk composition. The

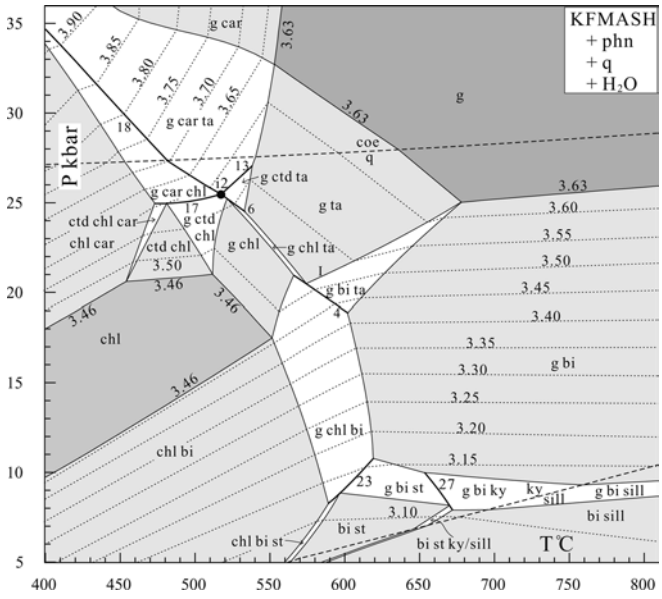

Fig. 10 P–T pseudosection in the KFMASH system, with phengite, quartz and H_2O in excess for a garnet–phengite–biotite gneiss (sample M4) from the Dabie Shan, Central China, with Al_2O_3:MgO:FeO:K_2O = 34.29:23.32:29.97:12.41, showing the invariant points (*closed circles*) and univariant reactions (*thick solid lines*) with labels the same as in Fig. 2 encountered by the bulk composition, divariant fields (*unshaded*), trivariant fields (*lighter-shaded*) and quadrivariant fields (*darker-shaded*). Isopleths of the Si content in phengite are shown as *dashed lines* with values (Si =)3.10–3.90 p.f.u.

phengite Si isopleths are shown in this pseudosection, where the Si contents rise clearly with pressure in the most trivariant and divariant fields but are effectively constant in the two quadrivariant fields chl + phn + q and g + phn + q/coe, with Si values of 3.46 and 3.63, respectively. The observed mineral assemblage for sample M4 is trivariant in the KFMASH system and takes up a wide P–T field with pressures ranging from about 10 to 25 kbar and temperatures over 600 °C. In this field, the Si isopleths in phengite are almost parallel to the temperature axis, being an optimal pressure indicator. The measured Si content of phengite in sample M4 is 3.30, which gives a pressure of about 15 kbar. It is obvious that the paragneisses with the present assemblage g + bi + phn + q represent a high-P but not ultrahigh-P metamorphism. If, as suggested by Wang and Liou (1991) and Liu et al. (2001), they did experience an ultrahigh-P metamorphic stage characteristic of the appearance of coesite, the possible mineral assemblage would be only the quadrivariant g + phn + coe.

Figure 11a and b show the T–X_{Mg} and P–X_{Mg} pseudosections for sample M4 calculated at P = 21 kbar and T = 580 °C, respectively. These pseudosections contain di-, tri- and quadrivariant fields which change with P, T and X_{Mg}. For example, as shown in Fig. 11a, the assemblage g + bi + phn + q corresponding to sample M4 will expand its stability field to lower T with X_{Mg} decreasing. Contours of the phengite Si content in Fig. 11b rise basically with pressure in the most

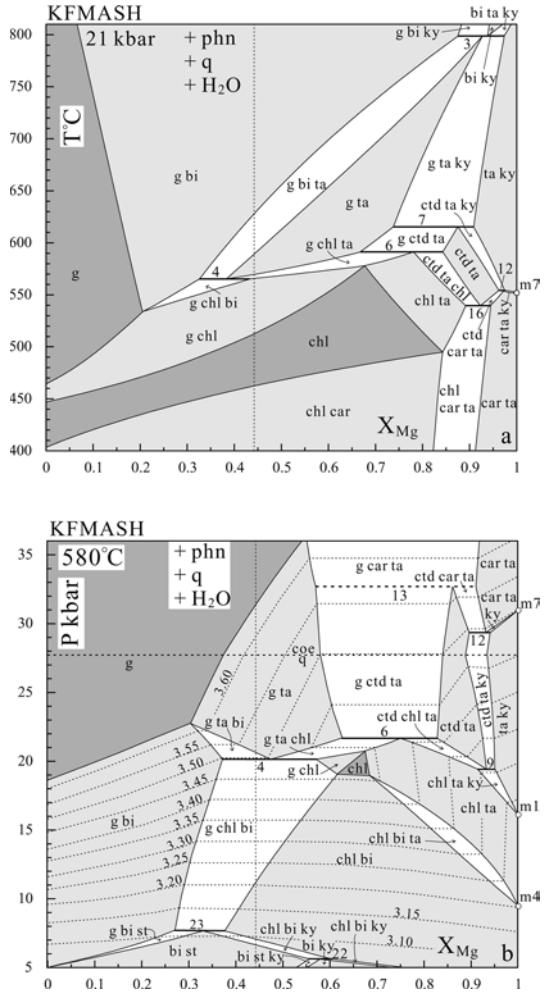

Fig. 11a, b T–X_{Mg} (**a**) and P–X_{Mg} (**b**) pseudosections at 21 kbar and 580 °C, respectively, in the KFMASH system with phengite, quartz and H_2O in excess for sample M4, showing the univariant reactions (*thick solid lines*) with labels the same as in Fig. 2 encountered by the bulk composition, divariant fields (*unshaded*), trivariant fields (*lighter-shaded*) and quadrivariant fields (*darker-shaded*). The subsystem reactions encountered by the bulk composition are denoted as *small open circles* and with labels the same as in Fig. 1. Isopleths of the phengite Si content are shown as *dashed lines* with values (Si =)3.10–3.60 p.f.u. in **b**. The *dashed line* in each diagram shows the X_{Mg} (= MgO/(MgO + FeO)) value for the bulk composition of sample M4

trivariant and divariant fields, are effectively constant in the two quadrivariant fields, and almost independent of pressure in the trivariant field chl–ta. These Si isopleths do not vary with X_{Mg} in any of the divariant fields, increase with X_{Mg} for most of the trivariant fields, decrease subtly with X_{Mg} in the trivariant field chl–bi, and decrease dramatically with X_{Mg} in the trivariant field chl–ta.

When compared with samples 7-37 and CHM39, sample M4 is richer in K and relatively poorer in Al and Mg. So, a prominent feature of the P–T, T–X_{Mg} and P–X_{Mg} pseudosections for sample M4 is that there are wide P, T and X_{Mg} ranges for the stability of biotite. Projection of the bulk composition of sample M4 on each AFM compatibility diagram is shown in Figs. 3 and 4 where the mineral assemblages for this sample correspond well with the assemblages in Fig. 10.

Discussion and conclusion

As mentioned-above, the calculated KMASH, KFASH and KFMASH system grids, and the pseudosections derived from them, are powerful in interpreting the high-P phase relations, P–T conditions, and also the variation of mineral composition such as the phengite Si contents with respect to P, T and X_{Mg} for a variety of pelitic compositions. However, additional system components such as CaO, Na_2O, MnO and Fe_2O_3 may differently influence some of the phase relationships discussed above. Adding CaO to the KFMASH system, the seven garnet-bearing invariant points presented in Table 1 and Fig. 2 would move along their garnet-absent reactions to lower pressure by about 1–4 kbar, such as the invariant points i1, i2, i4, i5, i7 and i8, or to lower temperature by about 20 °C, such as point i3, until the equilibria are joined by a Ca-bearing phase, zoisite or lawsonite. The only garnet-absent invariant point i6 is not changed by such an addition of Ca. With incorporation of Na into the KFMASH system, the basic KFMASH phase topology is not changed on addition of Na, neglecting the limited Na–K substitution in phengite and paragonite, until the equilibria are joined by a Na-phase, albite, paragonite, glaucophane or jadeite. Adding either CaO or Na_2O into the KFMASH system, however, it would cause much more complicated phase relations in the NKFMASH and CNKFMASH systems. Details will be discussed in subsequent papers.

Adding MnO expands the stability field of garnet to lower temperature and pressure, and adding Fe_2O_3 enlarges the stability of chloritoid, garnet and other KFMASH phases. However, both components are neglected by virtue of the lack of sufficient thermodynamic data for Mn and Fe^{3+} mineral end members.

High-P assemblages in metapelite

The unusual assemblages ky–ta and phn–ta have been emphasized as high-P indicators for pelitic compositions (e.g., Abraham and Schreyer 1976; Schreyer 1977; Chopin 1981; Schreyer 1988; Massonne and Schreyer 1989; Izadyar et al. 2000). As has been demonstrated, these assemblages are restricted to some unusual pelitic compositions poor in Fe which can be modeled in the MASH and KMASH systems. For example, in the pseudosections of the KMASH grid (Fig. 5a, b) there are wide P–T ranges for these unusual assemblages and, in the T–X_{Mg} and P–X_{Mg} pseudosections of the KFMASH grid in Figs. 7, 9 and 11, there is a stability field for ta + ky when X_{Mg} is greater than ~0.95. Decreasing X_{Mg} in a bulk composition favors the stability of chloritoid and garnet which would probably coexist with talc and phengite if

X_{Mg} is still relatively high, for instance, similar to that of sample 7-37. It is suggested here that the paragenesis ta–ctd, which is extensive in the high-P terranes from the Western Alps (Chopin 1981) and indicates pressures great than 19–20 kbar (above reaction 9 in Fig. 2) and temperatures between ~520 °C (over reaction 16) and 620 °C (below reaction 7), is more petrologically important than the ta–phn pair, although the latter has been highlighted by previous researchers (Abraham and Schreyer 1976; Chopin 1981; Massonne and Schreyer 1989; Izadyar et al. 2000). The paragenesis ta–ctd will give way to the assemblage g–ta–ky at $T > 600$–620 °C via reaction 7. For a bulk composition like sample 7-37, there is a wide P–T field for stability of the assemblage g–ta–ky in Figs. 6 and 7a, suggesting this would be a common assemblage for Mg-rich pelites at appropriate P and T. Such rocks have been reported from Tasmania (Råheim and Green 1974), northern Kazakhstan (Udovkina et al. 1977), and the Eastern Alps (Frank et al. 1987). Decreasing P–T, the paragenesis ta–ctd will be transformed into carpholite-bearing assemblages via reaction 16, or into a chl–ky assemblage through reaction 9. These assemblages were also reported by Theye et al. (1992) from Crete and the Peloponnese, and discussed by Schreyer (1988).

If the bulk compositions are rich in Al but poor in Mg, for instance, similar to sample CHM39, kyanite will be ubiquitous and would coexist, in the order of P and T rising along geotherms such as 8–10 °C/km, with carpholite, chloritoid and garnet in addition to phengite and quartz. Talc would be absent or limited to some specific P–T fields. If the bulk compositions are poor in both Al and Mg but relatively rich in Fe and K, for instance, analogous to sample M4, biotite will be pervasive and would coexist with only chlorite and garnet in addition to phengite and quartz, if the geothermal gradient is about 10 °C/km, and talc would occur only at lower geotherms such as 8 °C/km. In the latter case, if pressures are up to the stability field of coesite, the mineral assemblage would be only garnet + phengite + coesite for a rock with a bulk composition similar to that of sample M4.

According to the NFMASH grid of Guiraud et al. (1990), garnet and carpholite occur together under extremely high pressures ($P > 44$ kbar, $T < 600$ °C) which do not appear to occur in nature. However, the present study suggests that the g–car paragenesis can occur in nature if pressures are greater than only 25 kbar and temperatures lower than 550–600 °C in rocks relatively poor in Al, for instance, similar to samples 7-37 and M4 (see Figs. 6, 7b, 10 and 11b), and at pressures over 35 kbar and temperatures of about 560–600 °C in rocks like sample CHM39 rich in Al.

Phengite geobarometer

According to experimental calibrations of the phengite Si contents in the limiting KMASH assemblages (Massonne and Schreyer 1987, 1989; Massonne and Szpurka 1997), phengite shows a high potential for geobarometry. This has also been supported by the calculated results in this paper, namely, that phengite Si isopleths in various KMASH and KFMASH assemblages rise linearly with pressure, and moreover, these Si isopleths vary diversely with mineral assemblages both in slope and Si value. For example, as shown in Fig. 10, a phengite with Si = 3.40 coexisting with garnet–biotite or with chlorite–biotite would give rather different pressures.

Massonne and Szpurka (1997) proposed that at fixed P and T, the Si contents of KFASH phengite is lower than that in KMASH, and Bucher and Frey (1994) gave a contrasting prediction. From the present study, however, both conclusions would be possible. For example, at $P = 25$ kbar and $T = 650$ °C, the KMASH phengite coexisting with talc, kyanite and quartz would show Si = 3.40 from Fig. 5a, and the KFMASH phengite coexisting with talc, kyanite, garnet and quartz would have Si = 3.42 from Fig. 6, with the KMASH phengite increasing its Si content at fixed P and T as Fe^{2+} is incorporated. However, at $P = 16$ kbar and $T = 650$ °C, the KMASH phengite associated with talc, Mg-biotite and quartz will contain Si = 3.40 (Fig. 5b), and the KFMASH phengite coexisting with garnet, biotite and quartz will have Si = 3.32 (Fig. 10), with the KMASH phengite taking an opposite trend as Fe^{2+} is introduced. These complicated relationships between the Si content in phengite and X_{Mg} in bulk composition are clearly indicated in the P–X_{Mg} pseudosections shown in Figs. 7b and 9b. The phengite Si isopleths decrease with X_{Mg} in the trivariant fields with lower X_{Mg}, but increase clearly or subtly with X_{Mg} in the trivariant fields with higher X_{Mg}. In Fig. 11b, however, the phengite Si isopleths increase clearly with X_{Mg} in the trivariant fields with lower X_{Mg} values and, in the trivariant fields with higher X_{Mg} values, these Si isopleths decrease with X_{Mg} subtly or dramatically, or they increase with X_{Mg} clearly. As expected, mineral assemblages play the paramount role in governing the phengite composition.

Moreover, for the two phengite barometers proposed by Massonne and Schreyer (1989), that is, phengite coexisting with talc–kyanite–quartz/coesite (tks-phengite barometer) and with talc–phlogopite–quartz (tps-phengite barometer) in the KMASH system, both have been proved to be acceptable by the recalculation of Massonne and Szpurka (1997) using their newly derived thermodynamic data for phengite. However, the calculated phengite Si isopleths in this paper are in accordance with the experimentally well-constrained tks-phengite barometer, but in discordance with the experimentally poorly-constrained tps-phengite barometer which would overestimate pressures for the limiting assemblage. Rather than use these geobarometers, it is preferable to use pseudosections contoured for the Si content of phengite in the mineral assemblage of interest.

Acknowledgements This work was financially supported by the National Natural Science Foundation of China (grant number 40172031) and undertaken while C.J. Wei was a visitor in the School of Earth Sciences at the University of Melbourne. We are most grateful to D.J. Waters and C. Carson for helpful reviews of the manuscript.

Appendix

Mixing models, mineral and end-member formulae

Garnet (g): $[Mg, Fe]_3Al_2Si_3O_8$

A symmetric solution model is used for Mg–Fe mixing in binary garnet with the interaction parameter W(py, alm) = 2.5 kJ mol^{-1} following Dale et al. (2000).

End members

- Pyrope (py): $Mg_3Al_2Si_3O_8$
- Almandine (alm): $Fe_3Al_2Si_3O_8$

Chloritoid (ctd): $[Fe, Mg]Al_2SiO_5(OH)_2$

A symmetric solution model is used for Mg–Fe mixing in binary chloritoid with the interaction parameter W(mctd, fctd) = 1.0 kJ mol^{-1} following Holland and Powell (1998).

End members

- Mg-chloritoid (mctd): $MgAl_2SiO_5(OH)_2$
- Fe-chloritoid (fctd): $FeAl_2SiO_5(OH)_2$

Carpholite (car): $[Fe, Mg]Al_2Si_2O_6(OH)_4$

Mg–Fe mixing in carpholite is assumed to be ideal.

End members

- Mg-carpholite (mcar): $MgAl_2Si_2O_6(OH)_4$
- Fe-carpholite (fcar): $FeAl_2Si_2O_6(OH)_4$

Chlorite (chl): $[Fe, Mg]_4^{M2,3}[Mg, Fe, Al]_2^{M1,4}[Si, Al]_2^{T1}Si_2^{T2}O_{10}(OH)_8$

According to Holland et al. (1998), the thermodynamics of chlorite showing order-disorder in the KFMASH system are modeled using a quaternary symmetric mixing model. Interaction parameters are W(afchl, clin) = 18 kJ mol^{-1}, W(afchl, daph) = 14.5 kJ mol^{-1}, W(afchl, ames) = 20 kJ mol^{-1}, W(clin, daph) = 2.5 kJ mol^{-1}, W(clin, ames) = 18 kJ mol^{-1} and W(daph, ames) = 13.5 kJ mol^{-1}.

End members

- Al-free chlorite (afchl): $[Mg]_4^{M2,3}[Mg]^{M1}[Mg]^{M4}[Si]_2^{T1}[Si]_2^{T2}O_{10}(OH)_8$
- Clinochlore (clin): $[Mg]_4^{M2,3}[Mg]^{M1}[Al]^{M4}[Al]^{T1}[Si]^{T1}[Si]_2^{T2}O_{10}(OH)_8$
- Daphnite (daph): $[Fe]_4^{M2,3}[Fe]^{M1[Al]M4}[Al]^{T1}[Si]^{T1}[Si]_2^{T2}O_{10}(OH)_8$
- Amesite (ames): $[Mg]_4^{M2,3}[Al]^{M1}[Al]^{M4}[Al]_2^{T1}[Si]_2^{T2O}{}_{10}(OH)_8$

Phengite (phn): $K^{M1}[Fe, Mg, Al]^{M2A}[Al]^{M2B}[Si, Al]_2^{T1}Si_2^{T2}O_{10}(OH)_2$

Following Holland and Powell (1998), an ideal mixing model is used for phengite in the KFMASH system where mixing between Al, Mg and Fe is assumed only to occur in the M2A site and mixing of tetrahedral Al and Si is restricted to the two T1 sites.

End members

- Muscovite (mu): $K^{M1}[Al]^{M2A}[Al]^{M2B}Al^{T1}Si^{T1}Si_2^{T2}O_{10}(OH)_2$
- Celadonite (cel): $K^{M1}[Mg]^{M2A}[Al]^{M2B}Si_2^{T1}Si_2^{T2}O_{10}(OH)_2$
- Fe-celadonite (fcel): $K^{M1}[Fe]^{M2A}[Al]^{M2B}Si_2^{T1}Si_2^{T2}O_{10}(OH)_2$

Biotite (bi): $K[Fe, Mg]_2^{M2}[Fe, Mg, Al]^{M1}[Si, Al]_2^{T1}Si_2^{T2}O_{10}(OH)_2$

Following Powell and Holland (1999), ordered biotite in the KFMASH system is modeled with symmetric mixing and DQF models where Fe is assumed to favor the M1 site. Interaction parameters are W(phl, ann) = 9 kJ mol^{-1}, W(phl, east) = 10 kJ mol^{-1}, W(phl, obi) = 3 kJ mol^{-1}, W(ann, east) = −1 kJ mol^{-1}, W(ann, obi) = 6 kJ mol^{-1}, W(east, obi) = 10 kJ mol^{-1}, and a DQF parameter $I_{obi} = -10.73$ kJ mol^{-1}.

End members

- Phlogopite (phl): $K[Mg]_2^{M2}[Mg]^{M1}Al^{T1}Si^{T1}Si_2^{T2}O_{10}(OH)_2$
- Annite (ann): $K[Fe]_2^{M2}[Fe]^{M1}Al^{T1}Si^{T1}Si_2^{T2}O_{10}(OH)_2$
- Eastonite (east): $K[Mg]_2^{M2}[Al]^{M1}Al_2^{T1}Si_2^{T2}O_{10}(OH)_2$
- Ordered-biotite (obi): $K[Mg]_2^{M2}[Fe]^{M1}Al^{T1}Si^{T1}Si_2^{T2}O_{10}(OH)_2$

Talc (ta): $[Fe, Mg]_2^{M1}[Fe, Mg, Al]^{M3}[Si, Al]_2^{T1}[Si]_2^{T2}O_{10}(OH)_2$

Following Holland and Powell (1990, 1998), an ideal mixing model is used for the KFMASH ternary talc in which the Al is assumed to order onto the M3 site and to enter only the two T1 sites.

End members

- Talc (ta): $[Mg]_2^{M1}[Mg]^{M3}[Si]_2^{T1}[Si]_2^{T2}O_{10}(OH)_2$
- Fe-talc (fta): $[Fe]_2^{M1}[Fe]^{M3}[Si]_2^{T1}[Si]_2^{T2}O_{10}(OH)_2$
- Tschermak-talc (tats): $[Mg]_2^{M1}[Al]^{M3}[Al]^{T1}[Si]^{T1}[Si]_2^{T2}O_{10}(OH)_2$

Staurolite (st): $[Fe, Mg]_4Al_{18}Si_{7.5}O_{48}H_4$

A symmetric solution model is used for Mg–Fe mixing in binary staurolite with the interaction parameter $W(mst, fst) = -8.0$ kJ mol^{-1} following White et al. (2001).

End members

- Mg-staurolite (mst): $Mg_4Al_{18}Si_{7.5}O_{48}H_4$
- Fe-staurolite (fst): $Fe_4Al_{18}Si_{7.5}O_{48}H_4$

Single end-member minerals with unit activities

- Kyanite (ky) and sillimanite (sill): Al_2SiO_5
- Quartz (q) and coesite (coe): SiO_2

References

Abraham K, Schreyer W (1976) A talc-phengite assemblage in piemontite schist from Brezovica, Serbia, Yugoslavia. J Petrol 17:421–439

Albee AL (1965) A petrogenetic grid for the Fe-Mg silicates of pelitic schists. Am J Sci 263:512–536

Bucher K, Frey M (1994) Petrogenesis of metamorphic rocks. Springer, Berlin Heidelberg New York

Chopin C (1981) Talc-phengite: a widespread assemblage in high-grade pelitic blueschists of the western Alps. J Petrol 22:628–650

Chopin C (1984) Coesite and pure pyrope in high-grade blueschists of the Western Alps: a first record and some consequences. Contrib Mineral Petrol 86:107–118

Chopin C (1986) Phase relations of ellenbergerite, a new high-pressure Mg-Al-Ti silicate in pyrope-coesite-quartzite from the Western Alps. Geol Soc Am Mem 164:31–42

Chopin C, Schreyer W (1983) Magnesiocarpholite and magnesiochloritoid: two index minerals of pelitic blueschists and their preliminary phase relations in the model system MgO-Al_2O_3-SiO_2-H_2O. Am J Sci 283A:72–96

Dale J, Holland T, Powell R (2000) Hornblende-garnet-plagioclase-thermobarometry: a natural assemblage calibration of the thermodynamics of hornblende. Contrib Mineral Petrol 140:353–362

Frank W, Höck V, Miller C (1987) Metamorphic and tectonic history of the central Tauern window. In: Flügel HW, Faupl P (eds) Geodynamics of the Eastern Alps. Deuticke, Vienna, pp 34–54

Fransolet AM, Schreyer W (1984) Sudoite di/trioctahedral chlorite: a stable low-temperature phase in the system MgO-Al_2O_3-SiO_2-H_2O. Contrib Mineral Petrol 86:409–417

Guiraud M, Holland TJB, Powell R (1990) Calculated mineral equilibria in the greenschist-blueschist-eclogite facies in Na_2O-FeO-MgO-Al_2O_3-SiO_2-H_2O: methods, results and geological applications. Contrib Mineral Petrol 104:85–98

Harte B (1975) Determination of a pelitic petrogenetic grid for the eastern Scottish Dalradian. Carnegie Inst Washington Yearb 74:38–446

Harte B, Hudson NFC (1979) Pelitic facies series and the temperatures and pressures of Dalradian metamorphism in eastern Scotland. In: The Caledonides of the British Isles reviewed. Geol Soc Lond Spec Publ 8:323–337

Hess PC (1969) The metamorphic paragenesis of cordierite in pelitic rocks. Contrib Mineral Petrol 24:191–207

Holdaway MJ, Guidotti CV, Novak JM, Henry WE (1982) Polymetamorphism in medium- to high-grade pelitic metamorphic rocks, west-central Maine. Geol Soc Am Bull 93:572–584

Holland TJB, Powell R (1990) An enlarged and updated internally consistent thermodynamic dataset with uncertainties and correlations: the system K_2O-Na_2O-CaO-MgO-MnO-FeO-Fe_2O_3-Al_2O_3-TiO_2-SiO_2-C-H_2-O_2. J Metamorph Geol 8:89–124

Holland TJB, Powell R (1998) An internally consistent thermodynamic data set for phases of petrological interest. J Metamorph Geol 16:309–343

Holland T, Baker J, Powell R (1998) Mixing properties and activity-composition relationships of chlorites in the system MgO-FeO-Al_2O_3-SiO_2-H_2O. Eur J Mineral 10:395–406

Izadyar J, Hirajima T, Nakamura D (2000) Talc-phengite-albite assemblage in piemontite-quartz schist of the Sanbagawa metamorphic belt, central Shikoku, Japan. Island Arc 9:145–158

Kulke H, Schreyer W (1973) Kyanite-talc-schist from Sar E Sang, Afghanistan. Earth Planet Sci Lett 18:324–328

Labotka TC (1981) Petrology of an andalusite-type regional metamorphic terrane, Panamint Mountains, California. J Petrol 22:261–296

Liou JG, Wang Q, Zhang RY Cong B (1995). Ultrahigh-*P* metamorphic rocks and their associated lithologies from the Dabie Mountains, Central China. Field trip guide 3rd Int Eclogite Field Symp. Chinese Sci Bull 40(suppl):1–40

Liu JB, Ye K, Cong BL, Shegnori M, Fan HR (2001) Coesite inclusions in zircon from gneisses identified by laser Raman microspectrometer in ultra-high pressure zone of Dabie Mountains, China. Chinese Sci Bull 46:1912–1916

Massonne HJ (1989) The upper thermal stability of chlorite + quartz: an experimental study in the system MgO-Al_2O_3-SiO_2-H_2O. J Metamorph Geol 7:567–581

Massonne HJ, Chopin C (1989) PT-history of the Gran Paradiso (Western Alps) metagranites based on phengite geobarometry. In: Daly JS, Cliff RA, Yardley BWD (eds) Evolution of metamorphic belts. Geol Soc Spec Publ 42:545–549

Massonne HJ, Schreyer W (1987) Phengite geobarometry based on the limiting assemblages with K-feldspar, phlogopite and quartz. Contrib Mineral Petrol 96:212–224

Massonne HJ, Schreyer W (1989) Stability field of the high-pressure assemblage talc-phengite and two new phengite barometers. Eur J Mineral 1:391–410

Massonne HJ, Szpurka Z (1997) Thermodynamic properties of white micas on the basis of high-pressure experiments in the systems K_2O-MgO-Al_2O_3-SiO_2-H_2O and K_2O-FeO-Al_2O_3-SiO_2-H_2O. Lithos 41:229–250

Meyre C, Capitani C, Zack T, Frey M (1999) Petrology of high-pressure metapelites from the Adula Nappe (Central Alps, Switzerland). J Petrol 40:199–213

Powell R, Holland TJB (1990) Calculated mineral equilibria in the pelitic system. KFMASH (K_2O-FeO-MgO-Al_2O_3-SiO_2-H_2O). Am Mineral 75:367–380

Powell R, Holland TJB (1999) Relating formulations of the thermodynamics of mineral solid solutions: activity modeling of pyroxenes, amphiboles, and micas. Am Mineral 84:1–14

Powell R, Holland T, Worley B (1998) Calculating phase diagram involving solid solutions via non-linear equations, with examples using THERMOCALC. J Metamorph Geol 16:577–586

Råheim A, Green DH (1974) Talc-garnet-kyanite-quartz schist from an eclogite-bearing terrane, Western Tasmania. Contrib Mineral Petrol 43:223–231

Schreyer W (1977) Whiteschists: their compositions and pressure temperature regimes based on experimental, field and petrographic evidence. Tectonophysics 34:127–44

Schreyer W (1988) Experimental studies on metamorphism of crustal rocks under mantle pressures. Mineral Mag 52:1–26

Spear FS, Cheney JT (1989) A petrogenetic grid for pelitic schists in the system SiO_2-Al_2O_3-FeO-MgO-K_2O-H_2O. Contrib Mineral Petrol 101:149–164

Theye T, Seidel E, Vidal O (1992) Carpholite, sudoite and chloritoid in low-grade high-pressure metapelites from Crete and the Peloponnese, Greece. Eur J Mineral 4:487–507

Thompson JB Jr (1957) The graphical analysis of mineral assemblages in pelitic schists. Am Mineral 42:842–858

Udovkina NG, Muravitskaya GN, Laputina IP (1977) Talc-garnet-kyanite rocks of the Kokchetav block, Northern Kazakhstan (English translation). Dokl Akad Nauk SSSR 237:202–25

Vance D, Holland TJB (1993) A detailed isotopic and petrological study of a single garnet from the Gassetts Schist, Vermont. Contrib Mineral Petrol 114:101–118

Vrana S, Barr MWC (1972) Talc-kyanite-quartz schist and other high-pressure assemblages from Zambia. Mineral Mag 38:837–846

Wang X, Liou J G (1991) Regional ultrahigh-pressure coesite-bearing eclogitic terrane in central China: evidence from country rocks, gneiss, marble and metapellite. Geology 19:933–936

White RW, Powell R, Holland TJB, Worley B (2000) The effect of TiO_2 and Fe_2O_3 on metapelitic assemblages at greenschist and amphibolite facies conditions: mineral equilibria calculations in the system K_2O-FeO-MgO-Al_2O_3-SiO_2-H_2O-TiO_2-Fe_2O_3. J Metamorph Geol 18:497–511

White RW, Powell R, Holland TJB (2001) Calculation of partial melting equilibria in the system Na_2O-CaO-K_2O-FeO-MgO-Al_2O_3-SiO_2-H_2O (NCKFMASH). J Metamorph Geol 19:139–153

Xu G, Will TM, Powell R (1994) A calculated petrogenetic grid for the system K_2O-FeO-MgO-Al_2O_3-SiO_2-H_2O, with particular reference to contact-metamorphosed pelites. J Metamorph Geol 12:99–119